Energy Transport in a Concentrated Suspension of Bacteria

T. Ishikawa,[1] N. Yoshida,[1] H. Ueno,[2] M. Wiedeman,[3] Y. Imai,[1] and T. Yamaguchi[3]
[1]*Department of Bioengineering and Robotics, Tohoku University, Sendai 980-8579, Japan*
[2]*IAREO, Tohoku University, Sendai 980-8579, Japan*
[3]*Department of Biomedical Engineering, Tohoku University, Sendai 980-8579, Japan*
(Received 21 April 2011; published 7 July 2011)

Coherent structures appear in a concentrated suspension of swimming bacteria. While transport phenomena in a suspension have been studied extensively, how energy is transported from the individual cell scale to the larger mesoscale remains unclear. In this study, we carry out the first successful measurement of the three-dimensional velocity field in a dense suspension of bacteria. The results show that most of the energy generated by individual bacteria dissipates on the cellular scale. Only a small amount of energy is transported to the mesoscale, but the gain in swimming velocity and mass transport due to mesoscale coherent structures is enormous. These results indicate that collective swimming of bacteria is efficient in terms of energy. This paper sheds light on how energy can be transported toward smaller wave numbers in the Stokes flow regime.

DOI: 10.1103/PhysRevLett.107.028102 PACS numbers: 47.63.Gd, 47.57.E−, 47.63.mf, 87.18.Hf

The collective behavior of living creatures appears on various length scales, from bacteria to whales. Such behavior may be evolutionarily advantageous to members in terms of protection and mate choice [1,2]. The collective behavior of swimming fish and flying birds is advantageous in terms of energy saved, because the undulatory movements of leading animals generate thrust-type vortices that are shed into the wake [3,4]. Bacteria also exhibit collective swimming, and coherent structures appear in a concentrated suspension [5,6]. However, the collective swimming of bacteria is not in analogous to the collective behavior at high Reynolds number because of the dominant viscous effect. It would be interesting to clarify whether collective swimming of bacteria is advantageous in terms of energy saved.

In most three-dimensional (3D) flows, kinetic energy cascades from the large scale to smaller scales (i.e., from small to larger wave numbers). In a suspension of bacteria, the rotation of the flagella inputs energy into the system, which has a length scale in the nanometer range. Coherent structures, on the other hand, have a much larger length scale, of about 100 μm. In the Stokes flow regime, kinetic energy is not transported by convection, but dissipates instantaneously. It would be interesting to clarify how kinetic energy is transported towards smaller wave numbers even in a viscous-dominant system. While pattern formation and mass transport in a bacterial suspension have been studied extensively via experiments [7,8], continuum theories [9,10], and discrete numerical models [11–13], energy transport remains unclear [14].

In this Letter, we describe energy transport in a concentrated suspension of bacteria by measuring the 3D velocity field experimentally. Although it is very difficult to measure the velocity field in such a dense suspension, we successfully carried out the measurement using a confocal micro-PIV (particle image velocimetry) technique [15,16]. The results show that most of the energy input from the bacteria dissipates on the cellular scale, which differs from the former theoretical models, in which individual bacteria are treated as dipoles. Only a small amount of energy, on the order of about 0.1%, is transported from the individual cells to the mesoscale, but the gain in swimming velocity and mass transport is enormous. These results indicate that collective swimming of bacteria is efficient in terms of energy.

As a model bacterium, *Escherichia coli* (*E. coli*), wild-type strain MG1655, was used. *E. coli* has a cell body about 1 μm in diameter and 2 μm in length, and swims at a velocity of about 20 μm/s. The cells were grown for 12 h in tryptone broth (TB) [17] maintained at 37 °C, using a rotary shaker (160 rpm). Saturated cell culture (50 μL) was diluted in 5 mL of TB, and kept at 25 °C without shaking for 10 h. The cells were then separated from the media by centrifugation (2000 g, 10 min, 25 °C), washed with motility buffer MB+ [17], and finally suspended in MB+ with a cell density of 3×10^{10} cell/mL. The viscosity of MB+ at 25 °C is 9.8×10^{-4} Pa · s. To perform PIV analysis, tracer particles of diameter 1 μm (F13082, Molecular Probes, USA) were also suspended, with a number density of 5×10^9 bead/mL.

The confocal micro-PIV system [15,16] enabled us to measure the velocity field even inside the dense suspension, up to 50 μm from the glass wall, with high spatial and time resolution. These advantages enabled us to calculate the 3D flow field in the dense suspension, and discuss the wall effect on the coherent structures. The system consisted of an inverted microscope (IX71, Olympus, Japan), a confocal scanning system (CSU22, Yokokawa, Japan), a high-speed camera (Phantom v7.1, Vision Research, USA), a diode-pumped solid-state laser

(Laser Quantum, 532 nm, UK), a thermo plate (Tokai Hit, Japan), an objective lens (UPLSAPO, 20 ×, N.A. 0.75, Olympus, Japan), and a low-voltage piezoelectric translator controller (RT3D, Yokokawa, Japan).

A small drop of suspension, with a volume of 1 μL and a diameter of about 1 mm, was placed in a glass-bottomed Petri dish kept at 25 °C for the study. To avoid evaporative flows, a high humidity was maintained in the closed chamber by enclosing additional drops. Strong coherent structures were observed for many minutes, and the effect of bioconvection [18] was negligible in this small drop. Tracer movement was observed at the center of the drop in planes with $z = 10$, 20, 30, 40, and 50 μm. Here, the z axis was taken perpendicular to the wall, and fluid was present where $z \geq 0$. The x and y axes were parallel to the wall. We performed two kinds of measurements: (i) in-plane measurements, in which time-series images for PIV analysis were recorded in a fixed plane for 5 s (100 frames/s), and (ii) semi-3D measurements, in which measurements were carried out in five focal planes successively, using the piezoelectric translator, and images were recorded in each plane for 50 ms (5 frames) with a 250-ms interval. The PIV analysis was processed using interrogation windows of 16×16 pixels with 50% overlap (1 pixel = 1.15 μm). An iterative cross-correlation method was used to calculate the velocity field.

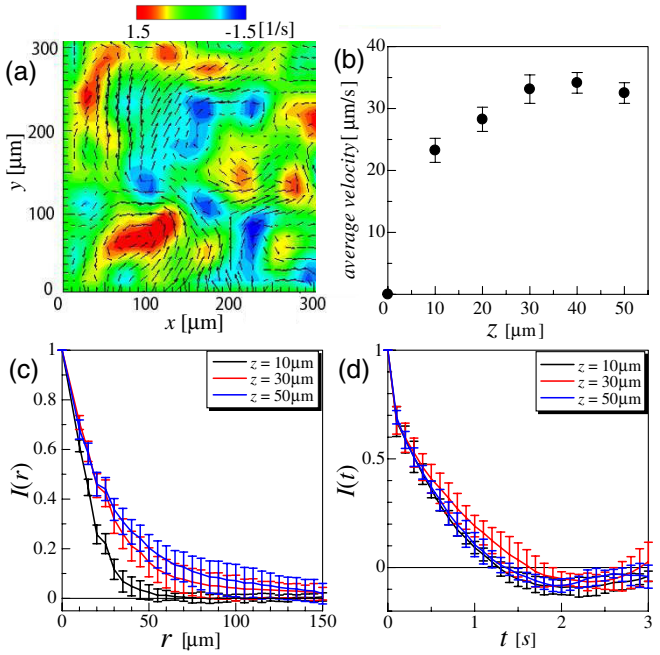

FIG. 1 (color online). Velocity field in the suspension: (a) a sample sequence of velocity vectors at $z = 30$ μm, where the color indicates the in-plane vorticity; (b) change in the average in-plane velocity with respect to depth, where the error bars indicate the standard deviation; (c) and (d) spatial and time correlations of the in-plane velocity vectors at three different planes ($z = 10$, 30, and 50 μm).

In the suspension, coherent structures similar to those reported in previous studies [5,6] were observed. Figure 1(a) shows a sample sequence of velocity vectors at $z = 30$ μm, where the color indicates the in-plane vorticity. The velocity field was measured by the motion of the tracer particles (not the bacteria), and thus the figure indicates the velocity of the solvent fluid (not the swimming velocity of the bacteria). We can see from Fig. 1(a) that vortices were generated on a scale much larger than that of the individual cells. Similar coherent structures were found in all focal planes ($z = 10$–50 μm). The average magnitude of the velocity vectors was calculated in each plane, and the results are shown in Fig. 1(b). The average velocity was saturated around $z = 30$ μm. Interestingly enough, strong coherent structures appeared even at $z = 50$ μm, indicating that the wall boundary was unimportant for these coherent structures. Previous experimental studies reported coherent structures in a thin film or at a fluid-solid interface. Thus, it was formerly unclear whether coherent structures appeared only when bacterial movement is restricted to two dimensions (2D). The present results indicate that this 2D restriction is unnecessary for coherent structures. The stability of the collective swimming may be maintained by limiting the surrounding space for bacteria to escape and by changing the orientation of the bacteria towards the extensional direction of the mesoscale flow field.

To clarify the scale of the collective motions, we calculated the spatial and time correlations of the velocities, defined in accordance with [11]. Figures 1(c) and 1(d) show the respective spatial and time correlations for $z = 10$, 30, and 50 μm. These results indicate that the length scale of the vortices increased with z, whereas the time scale was not much affected by z. Figure 1(d) also shows that the time scale of the velocity fluctuations was about 1 s. In our semi-3D measurements, two successive PIV measurements could be performed with an interval of 250 ms. Thus, by linearly interpolating two successive velocity fields, we were able to calculate the 3D distribution of the in-plane velocity at any time. Figure 2 shows the 3D distribution of the in-plane vorticity, where the isosurfaces indicate clockwise and counterclockwise rotation of a vortex, viewed from the bottom. We can see that the vortices grew in the z direction, and actually had 3D structure.

Calculating the 3D distribution of the in-plane velocity (v_x and v_y) is a major step towards obtaining the full 3D velocity field. By exploiting the continuity equation of an incompressible fluid ($\nabla . \boldsymbol{v} = 0$) and the no-slip boundary condition on the wall ($\boldsymbol{v}|_{z=0} = 0$), we can calculate v_z from

$$v_z = -\int_0^z \left(\frac{\partial v_x}{\partial x} + \frac{\partial v_y}{\partial y} \right) dz. \quad (1)$$

Equation (1) is solved numerically, using second-order finite differences for the differentials and the trapezoidal rule for the integral.

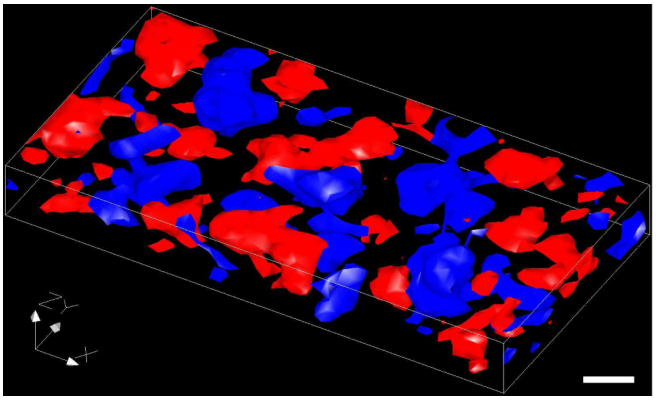

FIG. 2 (color online). Distribution of in-plane vorticity in three dimensions. Isosurfaces of 1.3 and -1.3 s^{-1} are shown, and the white scale bar is 50 μm.

Once the full 3D velocity field has been determined, the thrust force necessary to generate a coherent structure can be discussed. The velocity field obtained in this study may be regarded as a suspension average velocity, because the interrogation window of 18.4×18.4 μm is 1 order of magnitude larger than the cell body of *E. coli*, and the volume fraction of the bacteria is less than 10% (6% if the volume of an individual cell is assumed to be 2 μm^3). We further assume that the suspension is continuous, and the inertial and gravitational effects are negligible. Then, the momentum equation of the suspension is given by [19]:

$$\mu \nabla^2 \boldsymbol{v} = \nabla p - \nabla \cdot \Sigma^{(p)} = \boldsymbol{q}, \tag{2}$$

where μ is the viscosity, p is the pressure, $\Sigma^{(p)}$ is the particle stress tensor, and $\boldsymbol{q}$ is the thrust vector. Because p includes the isotropic contributions of the bacteria, and is not measured by the PIV analysis, it is placed on the right-hand side of Eq. (2).

Figure 3(a) shows one realization of the vector $\boldsymbol{q}$ at $z = 40$ μm, where the color indicates the magnitude of the in-plane velocity. We can see a strong correlation between the magnitudes of the vector $\boldsymbol{q}$ and the in-plane velocity. This indicates that the coherent structures are driven by the thrust force $\boldsymbol{q}$, which is generated by the divergence of the particle stress tensor. The magnitude of $\boldsymbol{q}$ varies with z, as shown in Fig. 3(b). Hence, a strong thrust force is generated even at $z = 40$ μm, where the wall effect is not very large. In the range $z = 10$–40 μm, the magnitude of $\boldsymbol{q}$ is about $0.4 - 0.5 \times 10^{-3}$ N/mL. By dividing this force by the number density of the bacteria (3×10^{10} cells/mL), we can deduce that individual bacteria contribute to the coherent structures by generating an average thrust force of about 0.01 pN/cell.

To discuss the efficiency of the bacteria in generating coherent structures, it is useful to compare the average value 0.01 pN/cell to the thrust force of a solitary bacterium swimming in a free space. Because it is difficult to

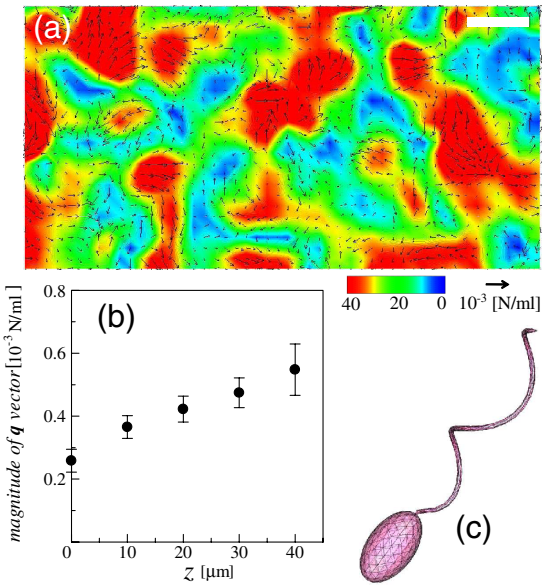

FIG. 3 (color online). Thrust force of the coherent structures: (a) one realization of the vector $\mathbf{q}$ distribution at $z = 40$ μm, where the arrows indicate $\mathbf{q}$ (the length scale is shown at the bottom), the color or shading indicates the magnitude of the in-plane velocity (μm/s), and the white bar indicates the 50 μm scale; (b) change in the magnitude of plane-averaged $\mathbf{q}$ with respect to depth; (c) computational mesh of the model bacterium used in the boundary element analysis, where 754 triangles are generated on the surface.

measure the thrust force experimentally, we employ a boundary element analysis. The details of the numerical methods were reported in our earlier study [17], in which the accuracy of the model was confirmed by comparison with experimental results for a solitary *E. coli* swimming near a wall. Figure 3(c) shows the computational mesh for the model bacterium used in this study. The cell body is an ellipsoid with major and minor axes of 2 and 1 μm, respectively, and the flagella length is 6 μm. Force-free and torque-free swimming is simulated in a fluid with viscosity 9.8×10^{-4} Pa · s. By rotating the flagellum relative to the cell body at a frequency of 100 Hz, the model bacterium swims at a velocity of about 19 μm/s. On the other hand, if the model bacterium stops swimming and is towed passively in the orientation direction at the same velocity, a thrust force of about 0.36 pN is necessary. Thus, one may assume that the thrust force of a free-swimming *E. coli* is about 0.36 pN. These results indicate that only a small amount of the individual thrust force contributes to the generation of coherent structures. Because the bacteria generate a mesoscale velocity greater than 40 μm/s [cf. Figure 3(a)], the maximum swimming velocity of the bacteria relative to the fixed coordinate system exceeds 60 μm/s. It follows that bacteria can attain a high swimming velocity, even though only a small amount of thrust force is used. Collective swimming of bacteria is therefore advantageous for achieving a high swimming velocity.

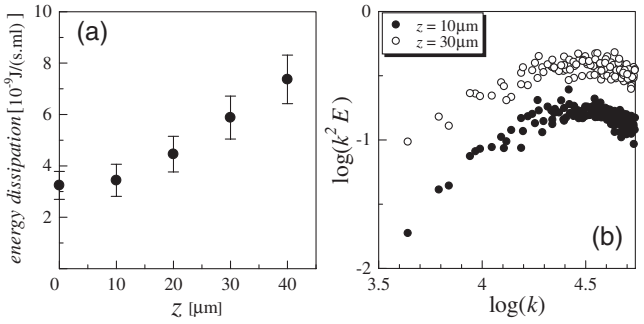

FIG. 4. Energy dissipation of the mesoscale velocity field: (a) change in the energy dissipation with respect to depth; (b) spectrum of k^2E at $z = 10$ and 30 μm.

Next, we discuss energy dissipation defined by $\nu|\mathrm{rot}\boldsymbol{v}|^2$, where ν is the kinetic viscosity. We first calculate the energy dissipation of the coherent structures using the velocity vectors obtained from the PIV analysis. The results are shown in Fig. 4(a). In the range $z = 10$–40 μm, the energy dissipation is about 3–7×10^{-9} J/(s · mL). In the Stokes flow regime, kinetic energy is not transported by convection, but dissipates instantaneously. Thus, the energy dissipation should balance the energy input from the bacteria at all wave numbers. That is, energy dissipation of 3–7×10^{-9} J/(s · mL) must be input by the bacteria via the mesoscale thrust force $\boldsymbol{q}$. This can be roughly verified by multiplying a thrust force of 0.4–0.5×10^{-3} N/mL by an average velocity of 30 μm/s, because the product has the same order of magnitude, 10^{-9} J/(s · mL).

By dividing the energy dissipation by the number density of the bacteria, we can deduce that individual bacteria dissipate energy at an average of about 1–2×10^{-19} J/(s · cell) on the mesoscale. We compared this value to the energy input from a solitary bacterium swimming in a free space, using the same boundary element analysis, and found that the model bacterium dissipates energy at about 3.9×10^{-16} J/s. The portion of its energy consumption that directly contributes to swimming can be approximated at 6.8×10^{-18} J/s, by multiplying the thrust force of 0.36 pN by the swimming velocity of 19 μm/s. Thus, the swimming efficiency of a solitary cell is about 2%. The value of 1–2×10^{-19} J/(s · cell) is less than 0.1% of the total energy input from the individual bacteria. These results indicate that the additional energy dissipation due to the coherent structures is small compared with the energy required for bacterial swimming.

Energy transport in a bacterial suspension is totally different from energy transport in a suspension of force-dipole particles, which has been used extensively in previous theoretical and numerical studies. Figure 4(b) shows the spectrum of in-plane energy dissipation k^2E obtained from the PIV analysis, where k is the wave number, and E is the in-plane kinetic energy. Because the largest wave number in the figure corresponds to a wavelength of about 18 μm, the figure shows the spectrum in mesoscale. Theories that model a bacterium as a force-dipole particle predict mesoscale energy dissipation similar to that shown in Fig. 4(b), but completely neglect energy dissipation for large wave numbers. In real suspensions of bacteria, most of the energy dissipates in the large wave number regime. Thus, without taking into account higher multipoles, energy transport in a real suspension cannot be predicted accurately.

The coherent structures also enhance mass transport, as reported by [7,8]. The diffusion coefficient calculated from the present velocity field is of the order of 10^{-10} m^2/s, which can be larger than the Brownian diffusion of macromolecules. Thus, the collective swimming of bacteria is also advantageous for enhancing mass transport in a suspension. This Letter demonstrates the advantages of collective swimming of bacteria, and sheds light on how energy can be transported toward smaller wave numbers in the Stokes flow regime.

We thank the National Institute of Genetics, Japan, for providing the bacteria. This work was supported by the NEXT program and Grant-in-Aids from JSPS.

[1] J. K. Parrish and L. Edelstein-Keshet, Science **284**, 99 (1999).
[2] D. J. T. Sumpter, Phil. Trans. R. Soc. B **361**, 5 (2006).
[3] D. Weihs, Nature (London) **241**, 290 (1973).
[4] H. Weimerskirch *et al.*, Nature (London) **413**, 697 (2001).
[5] N. H. Mendelson *et al.*, J. Bacteriol. **181**, 600 (1999).
[6] C. Dombrowski *et al.*, Phys. Rev. Lett. **93**, 098103 (2004).
[7] A. Sokolov *et al.*, Phys. Rev. Lett. **98**, 158102 (2007); A. Sokolov *et al.*, Phys. Rev. E **80**, 031903 (2009); A. Sokolov and I. S. Aranson, Phys. Rev. Lett. **103**, 148101 (2009).
[8] X.-L. Wu and A. Libchaber, Phys. Rev. Lett. **84**, 3017 (2000).
[9] R. A. Simha and S. Ramaswamy, Phys. Rev. Lett. **89**, 058101 (2002).
[10] D. Saintillan and M. J. Shelley, Phys. Rev. Lett. **100**, 178103 (2008); Phys. Fluids **20**, 123304 (2008).
[11] T. Ishikawa and T. J. Pedley, Phys. Rev. Lett. **100**, 088103 (2008); T. Ishikawa, J. T. Locsei, and T. J. Pedley, J. Fluid Mech. **615**, 401 (2008).
[12] J. P. Hernandez-Ortiz, C. G. Stoltz, and M. D. Graham, Phys. Rev. Lett. **95**, 204501 (2005); P. T. Underhill, J. P. Hernandez-Ortiz, and M. D. Graham, Phys. Rev. Lett. **100**, 248101 (2008).
[13] D. Saintillan and M. J. Shelley, Phys. Rev. Lett. **99**, 058102 (2007).
[14] T. Ishikawa, J. R. Soc. Interface **6**, 815 (2009).
[15] R. Lima *et al.*, Meas. Sci. Technol. **17**, 797 (2006); R. Lima *et al.*, Biomed. Microdevices **10**, 153 (2008).
[16] M. Saadatmand *et al.*, J. Biomech. **44**, 170 (2011).
[17] D. Giacche, T. Ishikawa, and T. Yamaguchi, Phys. Rev. E **82**, 056309 (2010).
[18] T. J. Pedley and J. O. Kessler, Annu. Rev. Fluid Mech. **24**, 313 (1992).
[19] G. K. Batchelor, J. Fluid Mech. **41**, 545 (1970).